IRAQI JOURNAL OF APPLIED PHYSICS
Vol. (14), No. (3), July-September 2018, pp. 35-40

Near-Edge X-ray Absorption Fine Structure Analysis of Magnesium-Palladium Nanoparticles Fabricated by Gas Evaporation Method

Tarek M. Radi
Ahmed A. Jasim
Ali H. Kadhum

Department of Physics, College of Science, University of Kerbala, Kerbala, IRAQ

The change of the chemical state of the Mg-Pd nanoparticles during hydro-/dehydrogenation has been investigated by the near edge x-ray absorption fine structure (NEXAFS) measurements under the in-situ condition. The Mg-Pd nanoparticles have been fabricated by the gas evaporation method using He gas and embedded in the fluorine resin in order to protect the Mg-Pd nanoparticles from the oxidation of the Mg-Pd nanoparticles. The Pd L_3-edge NEXAFS measurements have been carried out under the flowing the diluted hydrogen gas (4 wt% H_2) and pure He gas for the hydrogenation and dehydrogenation of the Mg-Pd nanoparticles, respectively. The in-situ Pd L_3-edge NEXAFS analyses have revealed that the Pd phases in the Mg-Pd nanoparticles are hydrogenated under the diluted hydrogen gas atmosphere. The subsequent dehydrogenation of the Pd phases has not been observed under the He gas. This result indicates that the dehydrogenation reaction of the Pd has been inhibited by the irreversible migration of the Mg toward the surface of the Mg-Pd nanoparticles.

Keywords: NEXAFS; Magnesium-Palladium structure; Nanoparticles; Dehydrogenation
Received: 28 May 2018, **Revised:** 31 July 2018; **Accepted**: 7 August 2018

1. Introduction

Methods for the synthesis of nanoparticles are taking place in other than gas-phase growth technology. However, gas-phase processing systems may have some advantages over other methods in some cases because of their following inherent advantages:

(a) Gas-phase processes are generally purer than liquid-based processes since even the most ultra-pure water contains traces of minerals, which seem to be avoidable today only in vacuum and gas-phase systems.

(b) Aerosol processes have the potential to create complex chemical structures which are useful in producing multicomponent materials, such as high-temperature superconductors [1].

(c) The process and product control is usually very good in aerosol processes.

(d) Being a non-vacuum technique, aerosol synthesis provides a cheap alternative to expensive vacuum synthesis techniques in thin or thick film synthesis [2]. Furthermore, the much higher deposition rate as compared to vacuum techniques may enable mass production.

(e) An aerosol droplet resembles a very small reactor in which chemical segregation is minimized, as any phases formed cannot leave the particle [3].

(f) Gas-phase processes for particle synthesis are usually continuous processes, while liquid-based synthesis processes or milling processes are often performed in a batch form. Batch processes can result in product characteristics which vary from one batch to another.

Hydrogen storage material is the essential component in the sustainable hydrogen energy system [4-7]. The role of the hydrogen storage material in the system is the storage tank of hydrogen which is the energy carrier between the electric energy supply and the energy consumer [8]. The properties required for the hydrogen storage material are high storage capacity and energetic efficiency i.e. the storage and release of the hydrogen under the low temperature and low pressure of hydrogen gas [9]. Magnesium (Mg) is the most promising material for the application of hydrogen storage because of high storage capacity up to 7.6 wt.% as a result of the hydrogenation of Mg. The problems of Mg for the practical use are the high temperature more than 350°C and high pressure of the hydrogen gas more than 3 MP during the hydro-/dehydrogenation reactions of Mg. These problems are caused by the low surface activity of Mg and the difficulty of the diffusion of hydrogen atoms thorough the Mg hydride (MgH_2) [10].

The nanoparticles composed of magnesium (Mg) and palladium (Pd) are expected to overcome the problems for the practical use of the Mg as the hydrogen storage materials [11]. The surface activity of Mg is improved by the deposition of transition metal atom on the surface of Mg. The Mg thin film

capped by Pd can uptake and release the hydrogen gas of 0.1 MPa under the room temperature because of the high hydrogen dissociation activity of Pd [12]. However, the diffusion length of hydrogen inside of the Mg bulk is limited by MgH_2 layer [10]. The scale-down of the size of Mg to nano-meter order is favorable for the further improvement of hydrogen diffusion kinetics [13-17].

In our previous work, the Mg-Pd nanoparticles have fabricated by the gas evaporation method using helium (He) gas [18]. The sizes of the Mg-Pd nanoparticles have distributed in the narrow range of 2-10nm. The hydrogen storage capacity of the Mg-Pd nanoparticles has been investigated by means of quartz crystal microbalance (QCM) technique [19,20]. Figure (1) shows the pressure-composition (P-C) isotherms for hydro/dehydrogenation of the Mg-Pd nanoparticles. The 1st plateau at ~0.3 Torr and the second one at ~60 Torr have been attributed to the hydrogen storage of Mg and Pd phases, respectively [21,22]. Although Mg-Pd NPs have been able to storage hydrogen up to 4.6 wt.% at the 1st hydrogenation, the release of hydrogen and 2nd hydrogen storage have not been observed in Fig. (1). It is considered that the change of the chemical state of the Mg-Pd nanoparticles has caused the degradation of the hydrogen storage capacity [23].

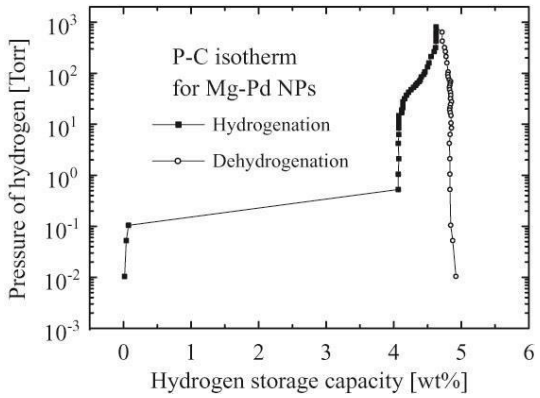

Fig. (1) The P-C isotherms for the hydro-/dehydrogenation of the Mg-Pd nanoparticles at 303K

In this study, we have investigated the chemical state of the Mg-Pd NPs by the near Pd L_3-edge X-ray absorption fine structure analysis (Pd L_3-edge NEXAFS). The NEXAFS measurements have been carried out under the *in-situ* condition. *In-situ* NEXAFS provides direct information on the change of the chemical state of the Mg-Pd NPs during the hydro-/dehydrogenation. Furthermore, the surface chemical state of the Mg-Pd NPs has been investigated by the x-ray photoelectron spectroscopy (XPS) method without the exposure of the Mg-Pd NPs to the air.

2. Experimental Part

The Mg-Pd nanoparticles were fabricated by the gas evaporation method using He gas (purity: 99.99995 %) [18]. The gas evaporation method is suitable for the fabrication of nanoparticles with clean surfaces i.e. absence of surfactants and contaminations. The rod shaped Mg and Pd wire were used as the evaporation sources. These sources were equipped in the same evaporation chamber and were evaporated simultaneously under 60 Torr of He gas. The Mg-Pd nanoparticles have been formed by the aggregation of the evaporated Mg and Pd atoms under the He gas atmosphere. The Mg-Pd nanoparticles were deposited on the Ni polycrystalline substrate and the polypropylene (PP) film (2.8 μm^t). Figure (2) shows the bright field image of the Mg-Pd nanoparticles obtained by the transmission electron microscopy (TEM). The average diameter of Mg-Pd nanoparticles was evaluated to be 5.9 nm. TEM bright field image in Fig. (2) reveals that Mg-Pd nanoparticles have been covered with oxide layer due to the air oxidation of Mg [22,24].

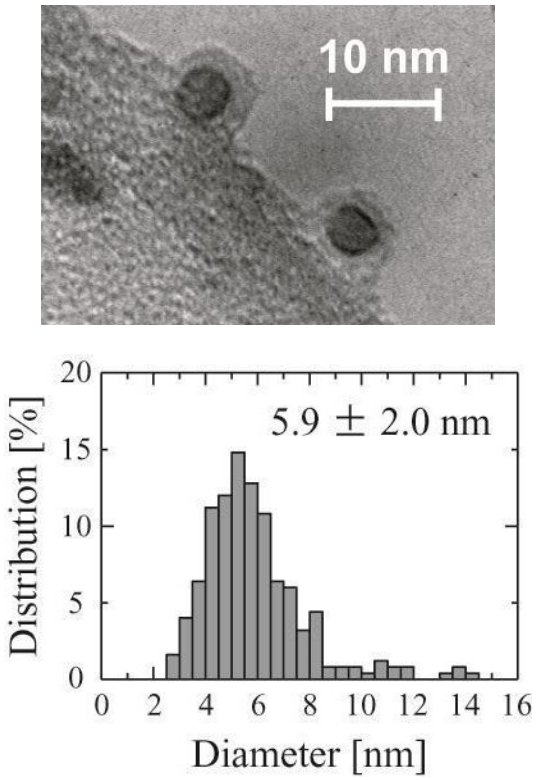

Fig. (2) The bright field image and the size distribution of the Mg-Pd nanoparticles

After the fabrication of the Mg-Pd nanoparticles, the fabrication chamber of the nanoparticles was evacuated to high vacuum of ~1×10^{-7} Torr. The Mg-Pd nanoparticles deposited on the Ni substrate were transferred to the ultra-high vacuum chamber (~5×10^{-10} Torr) for the XPS measurement. The XPS measurements were performed using Mg Kα X-ray (1253.6 eV) source and a hemispherical electron energy analyzer (PHOIBOS 100, SPECS GmbH). The XPS spectra were deconvoluted by using CasaXPS^{TM} software [25].

In order to avoid the air oxidation of the Mg-Pd nanoparticles, we attempted to cover the Mg-Pd nanoparticles with fluorine resin. The Mg-Pd nanoparticles deposited on the PP film were inserted into the transfer vessel [26] in the high vacuum. The transfer vessel enables us to transport the Mg-Pd nanoparticles sample to the glove box without the exposure to the air [27,28]. The Mg-Pd nanoparticles were covered with the fluorine resin under the nitrogen gas atmosphere in the glove box.

The Pd L_3-edge XAFS measurements using the synchrotron radiation were carried out at BL-10 of the SR center in Ritsumeikan University [26,29]. A Golovchenko-type double-crystal monochromator with Ge(111) was used for the monochromatization of incident X-ray. The Pd L_3-edge XAFS measurements were carried out with fluorescence x-ray yield method in flowing the dilute hydrogen gas (4 wt.% H_2) for hydrogenation (100cc/min) or He gas for dehydrogenation (500cc/min). The acquisition time of the NEXAFS spectrum was 3.5 minutes.

3. Results and Discussion

Figure (3) shows XPS spectrum for Mg 2p and Pd $3d_{5/2}$ core electrons of the Mg-Pd nanoparticles. It is noted that Pd 4p spectrum is observed around the energy region of Mg 2p spectrum when the both Mg and Pd atoms are contained on the surface of the sample. We have attempted the subtraction of the Pd 4p spectrum for the metallic Pd from the XPS spectrum around the energy range of 42~62 eV in order to derive the Mg 2p spectrum. Prior to the subtraction, the Pd 4p spectrum is normalized with respect to the peak area ratio of the Pd 3d spectra between the Mg-Pd nanoparticles and the metallic Pd. The Mg 2p spectrum has been obtained as the residual spectrum and deconvoluted into two components. The peak locating at 50.9 eV in Fig. (3) represents Mg^{2+} associated with MgO or $Mg(OH)_2$. The surface of the Mg-Pd nanoparticles has been oxidized by the residual gas such as O_2 and/or H_2O in the vacuum chamber. The peak locating at 49.5eV represents the chemical state of the Mg-Pd alloy. We have not been able to deconvolute the Mg 2p spectrum with the peak associated with the metallic Mg (49.7eV). The slight energy difference of the peak top positions between metallic Mg and the Mg-Pd alloy indicates that the valence electrons have been transferred from Pd atoms to Mg atoms in the Mg-Pd nanoparticles.

The transfer of the valence electrons is also indicated in the Pd $3d_{5/2}$ spectrum. The peak top of Pd $3d_{5/2}$ spectrum for the Mg-Pd nanoparticles obviously shifts to higher binding energy side by about 0.8eV. This energy shift is consistent with that of the Mg 2p spectrum. The Pd $3d_{5/2}$ spectrum for the Mg-Pd nanoparticles can be deconvoluted into two components of the metallic Pd (335.5eV) and the Mg-Pd alloy (336.3eV). The Pd $3d_{5/2}$ peak associated with PdO (336.9eV [30,31]) has not been observed in the spectrum of the Mg-Pd nanoparticles.

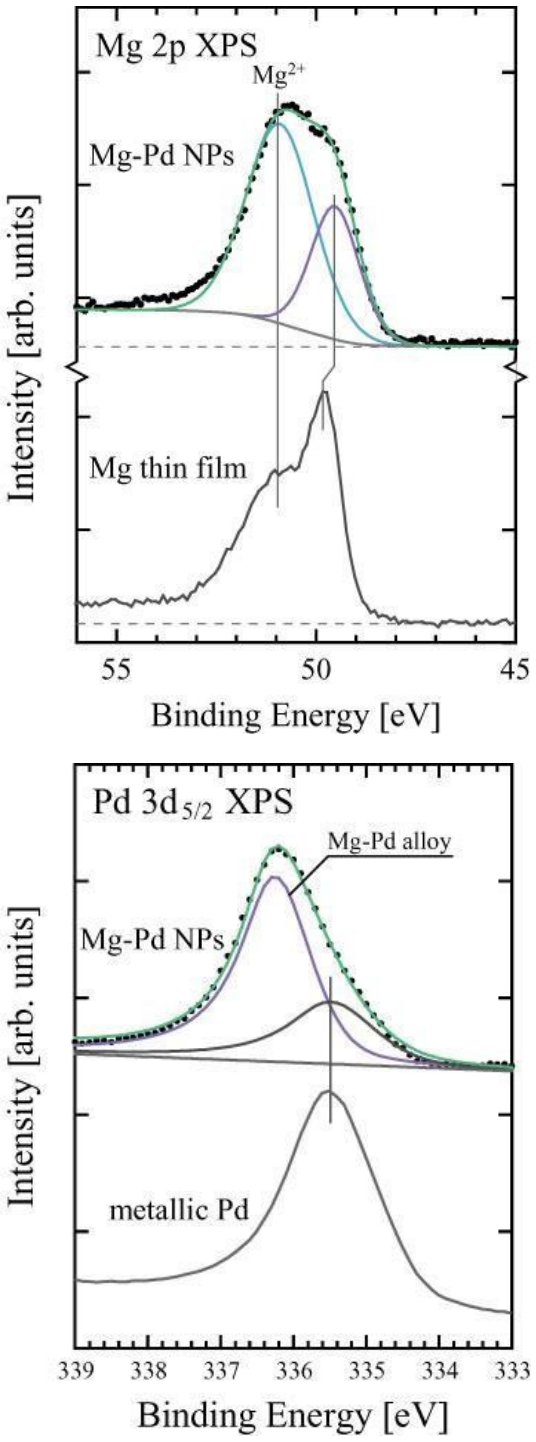

Fig. (3) The XPS spectra for the Mg 2p and Pd $3d_{5/2}$ core electrons of the Mg-Pd nanoparticles. The XPS spectra of the metallic Mg and Pd are shown as the standard spectra. The Mg 2p spectrum of the Mg-Pd nanoparticles has been obtained by subtraction of Pd 4p spectrum

We have demonstrated the *in-situ* NEXAFS measurement system with the Pd nanoparticles. Figure (4) shows the Pd L_3-edge NEXAFS for the Pd nanoparticles during hydro-/dehydrogenation.

The Pd nanoparticles have been covered with the fluorine resin prior to the NEXAFS measurement. The hydrogenation and dehydrogenation have been achieved by the exposure to the diluted hydrogen gas and He gas, respectively. The gradual change of the NEXAFS spectrum for the Pd nanoparticles can be seen in Fig. (4) during the hydro-/dehydrogenation. The peak top shifts toward higher energy side and the peak structure (3182eV) associated with Pd-H anti-bonding state grows gradually with the progress of the hydrogenation. The changes of the NEXAFS spectrum are reversed by the dehydrogenation. These results reveal clearly the reversibility of the hydrogenation reaction of the Pd nanoparticles.

Figure (5) shows the change of Pd L_3-edge NEXAFS spectrum for the Mg-Pd nanoparticles during the hydro-/dehydrogenation. The shape of the NEXAFS spectrum for the Mg-Pd nanoparticles before hydrogenation is quite different from that of Pd nanoparticles. The two peak structures are seen in the NEXAFS spectrum for the Mg-Pd nanoparticles. The first peak structure around 3176eV is attributed to the chemical state of the metallic Pd and the second one is attributed to that of the Mg-Pd alloy. The first peak structure in the spectrum for the Mg-Pd nanoparticles shifts slightly to the higher energy side compared with that of pure metallic Pd (3175eV) because of the overlapping partly with the peak structures for the Mg-Pd alloy [18].

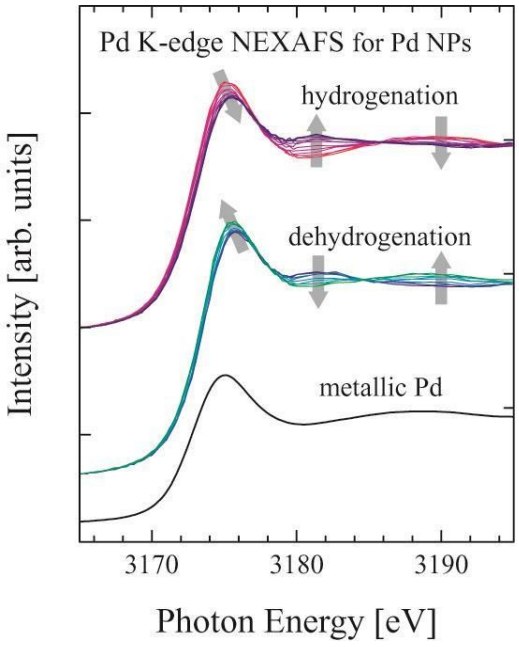

Fig. (4) The change of the Pd L_3-edge NEXAFS for the Pd nanoparticles during the hydro- /dehydrogenation. The spectrum of the metallic Pd is shown as the standard

The peak structures of the NEXAFS spectra for the Mg-Pd nanoparticles shift gradually with the progress of the hydrogenation. This peak shifts indicate the hydrogenation of the Pd or the change of the chemical state of the Mg-Pd alloy. In order to investigate the peak shift, the NEXAFS spectra in Fig. (5) have been simulated by the linear combination fitting. The fittings have been carried out with the NEXAFS spectra for the Mg-Pd nanoparticles before hydrogenation, Pd nanoparticles before hydrogenation and hydrogenated Pd nanoparticles. Figure (6) shows the simulation of the NEXAFS spectrum for the fully hydrogenated Mg-Pd nanoparticles. The NEXAFS spectrum of the Pd nanoparticles has been subtracted from that of the Mg-Pd nanoparticles. The NEXAFS spectrum of the hydrogenated Pd nanoparticles has compensated for the decline of the intensity. Figure (7) shows the variation of the fraction of each component during the hydrogenation of Mg-Pd nanoparticles. The gradual decrease and increase of the fraction of the Pd nanoparticles and hydrogenated Pd nanoparticles are clearly shown, respectively. The fraction of the initial Mg-Pd nanoparticles is constantly about 1, which means that the fraction of the Mg-Pd alloy has not changed during the hydrogenation.

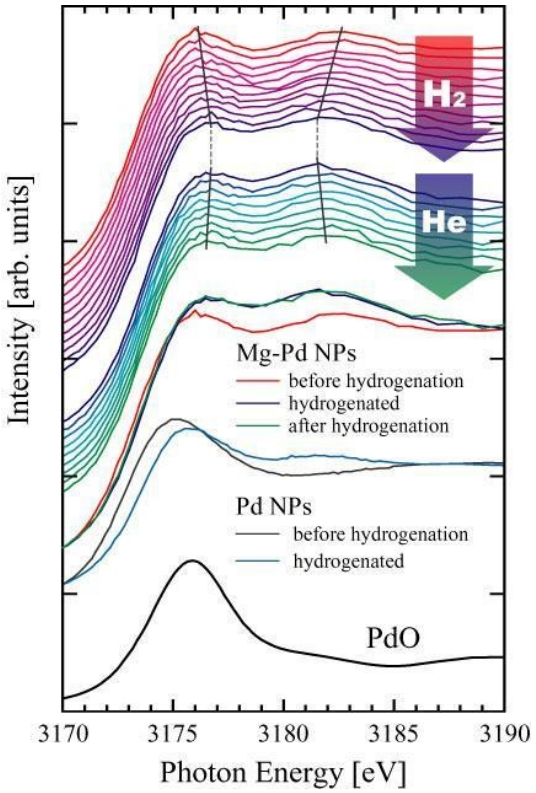

Fig. (5) The change of the Pd L_3-edge NEXAFS for the Mg-Pd nanoparticles during the hydro-/dehydrogenation. The spectra of the Mg-Pd nanoparticles and Pd nanoparticles before hydrogenation or hydrogenated are also shown. The spectrum of the PdO is shown as the standard

During dehydrogenation, the two peak structures in the NEXAFS of the Mg-Pd nanoparticles slightly shift toward the each initial energy positions. However, the complete dehydrogenation has not been observed in Fig. (5). This result indicates that the Pd phase has not been dehydrogenated under the

He gas atmosphere. The Pd phase in the Mg-Pd nanoparticles has been hydrogenated under the even if diluted hydrogen gas atmosphere. Figure (5) represents that the hydrogenated Pd phase has remained under the He gas. The remained hydrogenated Pd in the Mg-Pd nanoparticles suggests that a part of Pd phases is surrounded by the MgH_2 layers during the hydrogenation. Hydrogen atoms can be easily absorbed and desorbed via the uncovered Pd surface at the room temperature [12]. However, the covered Pd surface by the envelope with the low hydrogen diffusion property such as MgH_2 cannot release the hydrogen due to the inhibition of the hydrogen diffusion thorough the envelope. The MgH_2 layer might be migrated toward the surface of the Mg-Pd nanoparticles during the hydrogenation by the Kirkendall effect [32]. The affinity of interaction between Mg and hydrogen can cause the diffusion of Mg atoms. The mixture of Mg and Pd phases is favorable for the hydrogenation of Mg. However, it cannot play a role in the dehydrogenation of the MgH_2 [33].

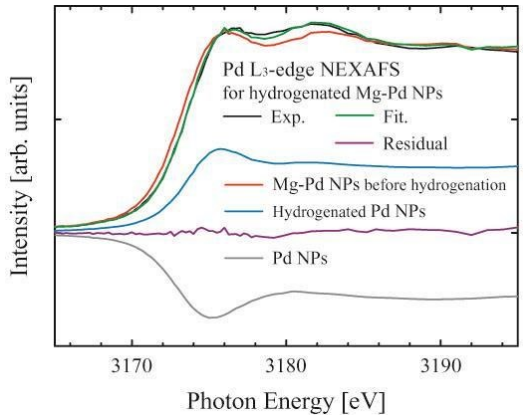

Fig. (6) The simulation of the Pd L_3-edge NEXAFS of the Mg-Pd nanoparticles after hydrogenation by the linear combination fitting

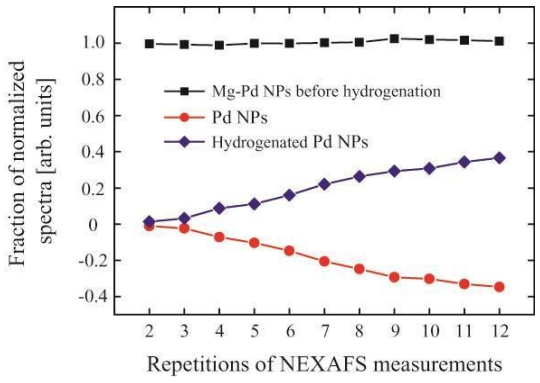

Fig. (7) The fraction of the normalized spectra for the components in the simulated spectra

4. Conclusions

The Mg-Pd nanoparticles have been fabricated by the gas evaporation method with He gas and investigated by XPS and *in-situ* Pd L_3-edge NEXAFS measurements. Both XPS and NEXAFS analyses indicate that the Mg-Pd nanoparticles are composed of the metallic Pd and the Mg-Pd alloy phases. The valence electron of the Pd is transferred to the Mg in the alloy phase. The hydrogenation of the Pd phase has been seen clearly by the *in-situ* NEXAFS measurements. On the other hand, the subsequent dehydrogenation of the Pd phase has not been observed under the He gas atmosphere, although the dehydrogenation of the pure Pd nanoparticles has been confirmed at the same condition. The inhibition of the dehydrogenation implies that the Pd phase on the Mg-Pd nanoparticles has been covered with the MgH_2 layer. The both hydrogen dissociation and recombination reactions occur on the Pd surfaces. The covering MgH_2 layer has prohibited these reactions on the surface of the Mg-Pd nanoparticles.

References

[1] T.T. Kodas, E.M. Engler and V.Y. Lee, Appl. Phys. Lett. 54, 1923-1925 (1989).
[2] X.W. Wang, H.H. Zhong and R.L. Snyder, Appl. Phys. Lett. 57, 1581-1583 (1990).
[3] F.E. Kruis, H. Fissan and A. Peled, J. Aerosol Sci., 29(5/6) 511-535 (1998).
[4] O.A. Hamadi, K.Z. Yahiya and O.N.S. Jassim, J. Semicond. Sci. Technol., 5(3) 182-186 (2005).
[5] K.S. Khashan and O.A. Hamadi, Eng. Technol. J., 25(2) 168-175 (2007).
[6] O.A. Hamadi, Iraqi J. Appl. Phys. Lett., 1(2) 3-8 (2008).
[7] O.A. Hamadi, B.A.M. Bader and A.K. Yousif, Eng. Technol. J., 26(8) 995-1001 (2008).
[8] A.A. Hadi and O.A. Hamadi, Iraqi J. Appl. Phys. Lett., 1(2) 23-26 (2008).
[9] A.K. Yousif and O.A. Hamadi, Bulg. J. Phys., 35(3) 191-197 (2008).
[10] I.P. Jain, C. Lal, A. Jaini, *Int. J. Hydro. Ener.*, 2010, 35, 5133.
[11] O.A. Hamadi, N.J. Shakir, F.H. Hussain, Bulg. J. Phys., 37(4), 223-231 (2010).
[12] K. Yoshimura, Y. Yamada, M. Okada, *Surf. Sci.*, 2004, 566-568, 751.
[13] O.A. Hamadi, Iraqi J. Appl. Phys. Lett., 3(1) 23-26 (2010).
[14] O.A. Hammadi and N.E. Naji, Iraqi J. Appl. Phys., 10(2) 27-31 (2014).
[15] O.A. Hammadi, W.N. Raja, M.A. Saleh and W.A. Altun, Iraqi J. Appl. Phys., 12(3), 35-42 (2016).
[16] O.A. Hammadi, W.N. Raja, M.A. Saleh and W.A. Altun, Iraqi J. Appl. Phys., 12(4), 19-28 (2016).
[17] O.A. Hammadi, J. Optoelectron. Phot., 7(5), 21 (2016).
[18] S. Ogawa, T. Mizutani, M. Ogawa, C. Yogi, T. Ohta, T. Yoshida, S. Yagi, *Confer. Proc. NANOCON 2012*, 2012, ISBN 978-80-87294-32-1, 274.

[19] V. Tsionsky and E. Gileadi, *Langmuir*, 1994, 10, 2830.
[20] I. Kulchytskyy, M. G. Kocanda and T. Xu, *Appl. Phys. Lett.*, 2007, 91, 113507.
[21] C.-J. Chung, S.-C. Lee, J. R. Groves, E. N. Brower, R. Sinclair, B. M. Clemens, *Phys. Rev. Lett.*, 2012, 108, 106102.
[22] S. Ogawa, S. Murakami, K. Shirai, K. Nakanishi, C. Tsukada, T. Ohta and S. Yagi, *e-J. Surf. Sci. Nanotech.*, 2011, 9, 315.
[23] O.A. Hammadi, J. Laser Micro/Nanoeng., 11(6), 151 (2016).
[24] O.A. Hammadi, J. Biomed. Nanotechnol., 12(8), (2016).
[25] N. Fairley, CasaXPS Version 2.3.13 Dev22: Software package for data processing. http://www.casaxps.com
[26] K. Nakanishi, S. Yagi, and T. Ohta, *IEEJ Trans. EIS*, 2010, 130, 1762.
[27] O.A. Hamadi, Iraqi J. Appl. Phys., 12(2) 9-13 (2016).
[28] O.A. Hammadi, Photonic Sensors, 6(4) 345-350 (2016). DOI:
[29] K. Nakanishi, S. Yagi, T. Ohta, *AIP Conf. Proc.*, 2010, 1234, 931.
[30] S. Murakami, S. Ogawa, K. Shirai, C. Tsukada, S. Yagi, K. Nakanishi, T. Ohta, *e-J. Surf. Sci. Nanotech.*, 2011, 9, 438.
[31] O.A. Hammadi and N.E. Naji, Photonic Sensors, 8(1) 43-47 (2018).
[32] G. Krishnan, B. J. Kooi, G. Palasantzas, Y. Pivak,and B. Dam, *J. Appl. Phys.*, 2010, 107, 053504.
[33] A. Baldi, M. Gonzalez-Silveira, V. Palmisano, B. Dam, R. Griessen, *Phys. Rev. Lett.*, 2009, 102, 226102.